# In situ polymer flocculation and growth in Taylor-Couette flows

SCHOLARONE™
Manuscripts

1

2

3

4

5

6

# In situ polymer flocculation and growth in Taylor-Couette flows

*Athena Metaxas,[1] Nikolas Wilkinson,[1] Ellie Raethke,[1] and Cari S. Dutcher[2,] \**

[1] Department of Chemical Engineering and Materials Science, University of Minnesota – Twin

Cities, 421 Washington Ave SE, Minneapolis, MN 55455, USA

[2] Department of Mechanical Engineering, University of Minnesota - Twin Cities, 111 Church

Street SE, Minneapolis, MN 55455, USA

*Corresponding Author Email: cdutcher@umn.edu

15

16

17

18

19

20

21

22

23

Keywords: flocculation, Taylor-Couette, mixing, radial fluid injection, bentonite, polyelectrolytes
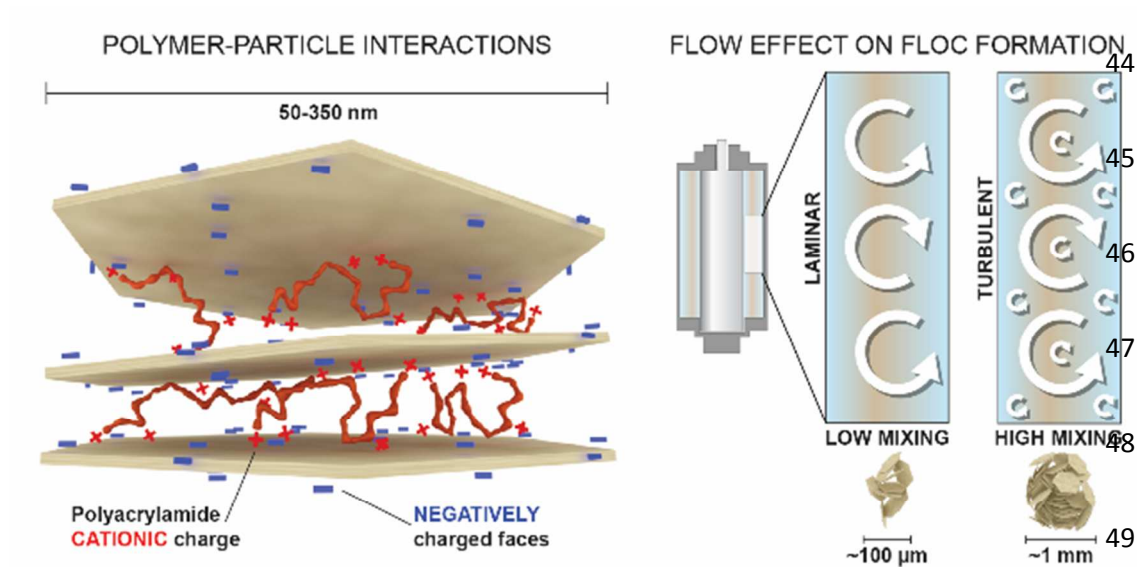
26 Abstract

27

28 Flocculation of small particulates suspended in solution is a key process in many industries,

29 including drinking water treatment. The particles are aggregated during mixing to form larger

30 aggregates, known as flocs, through use of a polyelectrolyte flocculant. The flocculation of these

31 particulates in water treatment, however, are subject to a wide spatial variation of hydrodynamic

32 flow states, which has consequences for floc size, growth rate, and microstructure. Floc assembly

33 dynamics are explored here using a commercially available cationic polyacrylamide, commonly

34 used in water treatment, and anisotropic Na-bentonite clay particles under a variety of

35 hydrodynamic mixing conditions. A Taylor-Couette cell with the unique ability to radially inject

36 fluid into the rotating annulus was used to study how specific hydrodynamic flow fields affect

37 assembly and structure of these materials during the flocculation process. Faster floc growth

38 rates and decreased floc fractal dimensions were observed for higher order flow states, indicating

39 improved mass transfer of the polymer flocculant and breakage at the edges of the flocs (shear

40 rounding), respectively. This work sheds more light on the complexities of polymer-induced

41 flocculation, towards improving dosing and efficiency of large-scale operations.

42

43   Graphical Abstract



POLYMER-PARTICLE INTERACTIONS

50-350 nm

Polyacrylamide / CATIONIC charge

NEGATIVELY charged faces

FLOW EFFECT ON FLOC FORMATION

LAMINAR

TURBULENT

LOW MIXING

HIGH MIXING

~100 µm

~1 mm

50   Graphical abstract sentence summary: Transient, in-situ polymer-particle flocculation and

51   growth was studied as a function of hydrodynamic flow state using a modified Taylor-Couette

52   cell.

53

54

55    1    Introduction

56

57        The removal of solid particulates using polyelectrolyte-driven flocculation is a common

58    process in a variety of applications including paper manufacturing and drinking water

59    treatment.[1–3] Despite its widespread use, the process remains poorly understood due to the

60    complexity of the system, and treatment plants therefore rely on highly empirical methods to

61    determine polymer flocculant dosing levels. Charged polymers are added to a fluid system

62    during mixing in order to bind to suspended particulates, forming flocs.  Rapid floc growth is

63    then enabled by orthokinetic aggregation, where the polymer-coated particulates collide due to

64    fluid motion, and the velocity gradient during the mixing process depends on the nature of the

65    fluid flow.[4–6] The local hydrodynamics around a growing floc is one of the key factors that

66    affects the conformation of the polymer on the surface. Extensional forces in particular can

67    stretch the polymer from the surface to lengths greater than the radius of gyration, $R_g$, of the free

68    polymer in solution, increasing the bridging capability of the polymer.[7,8] As the flocs are formed

69    and grow during the flocculation process, they can eventually break due to fluid shear forces.[9,10]

70    After some time, the flocs will approach a steady state between floc growth and breakage.[11–13]

71        There are several different molecular-level mechanisms for polymer-particle adsorption and

72    flocculation events, including charge neutralization, polymer bridging, charge-patch flocculation,

73    and polymer depletion.[1,3,14–16] The aqueous environment affects the underlying flocculation

74    mechanism through highly interrelated physicochemical properties including the suspension

75    composition (pH, ionic strength, and salt valency),[8] coagulant type,[17,18] particle surface

76    properties,[19] and dosing and mixing conditions.[9,12,20] In this study, bentonite was used as the

77    solid particulate of interest. Bentonite is an anisotropic smectite clay commonly found in surface

78    waters with a high adsorption capacity for water and has been used in other flocculation

79    studies.[21–24] Individual bentonite particles can be visualized as thin sheets with negatively

80    charged faces and either positively or negatively charged edges depending on the solution

81    pH.[25,26] As a result, bentonite sheets can be arranged in a porous, edge-face arrangement, an

82    edge-edge arrangement, or  a dense, face-face structure.[27,28] Variations in aggregate surface

83    morphology more than likely result in different polyelectrolyte adsorption capacities and

84    interaction potentials due to the uneven charge distribution of the functional edge groups.

85    These complex interdependencies on the floc assembly kinetics and final floc microstructure

86    are not well understood and can result in poorly optimized polymeric dosing, which is one of the

87    major technical issues treatment plants consider. Under-dosing results in insufficient particulate

88    removal and over-dosing results in particulate restabilization, both undesirable outcomes which

89    can be cost-prohibitive in water treatment.[29] Flocs fragmented resulting from of shear forces can

90    be re-suspended and are often more difficult to remove than the initial particulate. For optimal

91    separation, large hydrodynamically robust flocs are desired for flocs to readily settle out due to

92    gravity, as well as withstand turbulent stresses in the flow with little to no fragmentation.[1,10,30]

93    The effects of physicochemical and hydrodynamic conditions on final floc microstructure

94    have been examined using small angle light scattering, yielding final floc size and fractal

95    dimensions.[31–33] These studies found that the longer characterization length scales accessible by

96    static light scattering work well to determine mass fractal dimensions. However, interpretation of

97    the scattering patterns can be difficult, and static light scattering works best for smaller

98    aggregates with loosely packed structures. Recently, advanced image analysis techniques have

99    been used to study the dynamic flocculation behavior using jar tests and impellers, which offers a

100   more non-intrusive method of studying the flocs as compared to obtaining and preparing a

101    sample for light scattering experiments.[9] Jar tests replicate scaled-down industrial water

102    treatment conditions, but lack homogeneous spatial and temporal flow features that are needed to

103    precisely study floc strength as a function of hydrodynamic flow. In addition to the lack of varied

104    flow states, the shear stresses within the fluid cannot be accurately controlled in a jar test to

105    determine the point where floc breakage occurs.[30,34]

106         Unlike jar tests, Taylor-Couette (TC) cells, devices consisting of two concentric cylinders

107    with a specified gap width, offer an experimental method to study mixing events with the ability

108    to precisely control the hydrodynamics. TC cells can generate a wide variety of flow states as a

109    function of either or both cylinder speeds, and they range from laminar types to turbulent

110    types.[35–40] Four different flow states were used in this study in order of increasing inner cylinder

111    speed: 1) laminar Taylor vortex flow (LTV), 2) laminar wavy vortex flow (LWV), 3) turbulent

112    wavy vortex flow (TWV), and 4) turbulent Taylor vortex flow (TTV). Laminar Taylor vortex

113    flow consists of axisymmetric, toroidal vortices with a characteristic spatial frequency but no

114    temporal frequency whereas laminar wavy vortex flow consists of a characteristic temporal and

115    spatial frequency.[41] From a qualitative perspective, LTV flow look like a series of parallel bands

116    whereas LWV flow appears as parallel waves. The turbulent cases of these two flow states

117    physically resemble their laminar counterparts with additional turbulent features such as eddies.

118    The wide variety of flow states accessible by a TC cell, in addition to optical access via the

119    transparent outer cylinder has made it an ideal tool to study a variety of processes such as

120    polymer drag reduction, catalysis, filtration, and liquid-liquid mixing.[42–44] TC cells have also

121    been used to study flocculation, although prior studies with TC cells were limited in that flocs

122    had to be pre-formed outside of the cell.[10,45–47]

123     To study the entirety of the mixing process in an in-situ manner, a modified TC cell has

124     been designed and built by Wilkinson and Dutcher[48] to directly inject the polymer flocculant into

125     the annulus. Unlike other TC cells where the injection  was in a single location or protruded into

126     the annulus, the cell built by Wilkinson and Dutcher injects flocculant at multiple, precisely

127     spaced axial and azimuthal locations to allow for larger volume injections and smoothing of any

128     azimuthal concentration gradients.[43,48–50] The injection ports are built into the inner cylinder and

129     the port covers lie flush against the surface of the inner cylinder and are counter-matched to

130     prevent any alteration of the flow profile. Additional studies with this modified TC cell recently

131     published by Wilkinson and Dutcher have been conducted to determine the stability of flow

132     vortices to injection, and the flow states tested in this study are stable over a wide range of

133     cylinder speeds, injection drive pressures, and injection times.[51] The advantages that this

134     modified TC cell offers over other cell designs is the ability to explore initial mixing effects in

135     flocculation of bentonite clay with a polyelectrolyte flocculant. Optical access allows for image

136     analysis techniques to calculate the size, morphology, and growth rate of flocs in a precise

137     hydrodynamic flow state.


138     2    Materials and Methods

139

140         2.1    Materials

141         The polymer flocculant, or polyelectrolyte, used in this study is a commercially available

142     cationic polyacrylamide (FLOPAM FO 4190 SH, SNF Polydyne) with 10% quaternary amine

143     monomer charge groups and a molecular weight of $6 \times 10^6$ g/mol. A 0.2 wt% polymer solution

144     was made by using a Jiffy mixer attachment to mix the solid polymer pellets into distilled water

145     for 30 min. The polymer rested in a refrigerator overnight prior to use and was remade every 2

146    weeks as necessary per supplier instructions. The distilled water used is from Premium Waters,

147    Inc. Powdered Na-Bentonite is ACS grade from Fisher Scientific and was used as received.  The

148    kinematic viscosity of the 30 mg/L bentonite suspension was $1.00 \pm 0.05$ cSt from steady shear

149    experiments as shown in Figure S1, which showed Newtonian behavior in the frequency regions

150    relevant to the speeds tested in this study.

151        2.2   Methods: Sample Loading into TC Cell annulus and Spatial Calibration

152        The TC cell used in these experiments consist of a total of 16 injection ports evenly

153    distributed axially and azimuthally into the inner cylinder. Because the injection ports do not

154    protrude into the annulus and the port covers are contour-matched to the inner cylinder, the flow

155    profile of the resultant vortices are not modified during operation as shown by Wilkinson and

156    Dutcher.[48] Additional details on the TC cell design, with inner cylinder diameter of $13.5407 \pm$

157    0.0025 cm, gap width of 0.84 cm, inner cylinder radius to outer cylinder radius ratio of 0.891,

158    and injection assembly can be found elsewhere.[48] To make the bentonite suspensions, 30 mg of

159    bentonite was transferred to a 2 L beaker filled with 1 L of water. This process was repeated to

160    make a total of 2 L of 30 mg/L bentonite suspensions. The bentonite was dispersed using a

161    VELP Scientifica JTL4 Flocculator for 30 min at 300 RPM. The pH of the resultant suspensions

162    is approximately 6.6 due to the interaction of dissolved carbon dioxide in water and bentonite.[52]

163    Since the size and morphology of bentonite, an anisotropic particle, is dependent on solution

164    ionic strength and pH, respectively, these two parameters were kept consistent between all

165    experiments in this study.[53,54] Once finished, the bentonite suspensions were immediately

166    transferred to the annulus of the TC cell by way of tubing attached to the base of the cylinder

167    assembly as seen in Figure 1.

168        Once the bentonite was loaded, refractive index-matching paraffin oil was poured into the

169        Plexiglass tank holding the apparatus to eliminate the curved glass surface of the outer cylinder.

170        The cell was axially illuminated with a flicker-free LED light strip (Metaphase 19 in Exo2 Light)

171        to better visualize the injection port covers for spatial calibration for image analysis. A spatial

172        calibration image of the bottom-most port cover of the inner cylinder was captured using a

173        Basler Ace camera (1280 × 1024 pixels, 60 fps maximum frame rate) with a Tamron 25 mm c-

174        mount lens. ImageJ was then used to calculate the pixel-to-mm ratio of the spatial calibration

175        image.

176        2.3    Methods: Flocculation Experiment Protocol

177        The inner cylinder is rotated by a stepper motor (Applied Motion Products HT34-497 2 phase

178        stepper motor with a STAC5-S-E120 controller) equipped with a 7:1 gear reducer (Applied

179        Motion Products 34VL007) for inertial balance between the motor and the cylinder. To remove

180        unwanted flow dislocations in the vortices, flow priming was conducted by way of a motor

181        control script to ramp down from a speed higher than the required speed to the intended speed.[51]

182        A laser diode (Thorlabs, 450 nm, 1600 mW max) combined with a laser line generator was used

183        to create a laser light sheet tangential to the inner cylinder as shown in Figure 2A. The cationic

184        polyacrylamide injection process and movie recording were operated using LabView. For all

185        experiments, the drive pressure was set to 30 psi to inject cationic polyacrylamide from the

186        injection ports into the annulus at a calibrated injection rate of 1.115 g/s for 6 seconds as reported

187        in Wilkinson et al,[48] which corresponds to the optimal polymer dose for the bentonite-distilled

188        water of ~8 ppm as reported elsewhere.[53] The camera was vertically adjusted such that the field

189        of view was between the 3rd and 4th injection port covers from the bottom of the annulus. The

190        frame rate of the camera was set to 30 fps with an exposure time of 8 ms for all experiments.

191    As discussed later, flocculation mixing protocols typically have two speeds – an initial

192    "Mix speed" (Stage 1), followed by a slower "Growth Speed" (Stage 2).  However, it should be

193    noted that these standard names are misleading – certainly some growth can occur in the early

194    "Mix" stage, and mixing can occur in the later "Growth" stages. In this study, the early Stage 1

195    steady "Mix" speeds were $0.04$ s$^{-1}$, $0.17$ s$^{-1}$, $0.50$ s$^{-1}$, $1.10$ s$^{-1}$, and $1.47$ s$^{-1}$, and the later Stage 2

196    steady "Growth" speed is fixed at $0.46$ s$^{-1}$. After flow priming, the initial inner cylinder Stage 1

197    angular velocity was set and the recording started.  After a 30 second delay, the polymer was

198    injected and mixed at this Stage 1 speed for 3 min to distribute the polymer throughout the

199    annulus. After 3 min at the Stage 1 speed, the inner cylinder speed was then set to the Stage 2

200    speed of $0.46$ s$^{-1}$ at a quick ramp rate of $0.92$ rotations/s$^2$ for 30 min to allow the flocs to grow.

201    The value of $0.46$ s$^{-1}$ was chosen as it was the slowest speed tested which was able to suspend

202    enough flocs throughout the duration of the flocculation process for image analysis. Once each

203    experiment was completed, the annulus was drained and the inner cylinder removed from the

204    apparatus for cleaning with a dilute solution of Micro-90. The inner cylinder drive shaft and

205    ports were re-primed with cationic polyacrylamide. Once reassembled, the annulus was refilled

206    with distilled water prior to the next experiment.

207    2.4    Methods: Image Analysis of Flocculation Experiments

208    The movies were analyzed in MatLab using a process adapted from Vlieghe et al[10] to

209    obtain floc size and morphology information as a function of time. The raw images were

210    converted to grayscale images and binarized for all experiments as shown in Figure 2C. Size was

211    reported in terms of the radius of gyration, $R_g$, of the floc as calculated by the following equation,

$$R_g^2 = \frac{1}{N_p} \sum_{i=1}^{N_p} [(x_i - x_c)^2 + (y_i - y_c)^2] \quad \#(1)$$

212     where $N_p$ is the number of pixels making up each floc, $(x_i, y_i)$ are the individual pixel coordinate

213     pair, and $(x_c, y_c)$ is the centroid coordinate pair. The area average for all flocs in a 10 second

214     interval (300 frames) was computed.

215          To quantify the morphology of the flocs, a surface-based fractal dimension, $D_{sf}$, was

216     calculated using the following relationship as reported by Vlieghe et al[10]

$$A \propto P^{2/D_{sf}} \#(2)$$

217
218     where $A$ is the cross-sectional floc area, and $P$ is the floc perimeter. The fractal dimension varies

219     in value from 1 to 2, where a value of 1 indicates a circular shape and a value of 2 indicates a

220     rod-like shape. A linear regression was performed on each 10 second set of data $(A, P)$ to

221     determine $D_{sf}$.

222     3      Results and Discussion

223

224          3.1     Effect of Hydrodynamics on Floc Size and Growth Rate

225          In water treatment processes, it is preferable to rapidly mix the flocculant for a short

226     period of time with the solid particulate of interest to disperse the polymer throughout the

227     suspension as quickly and evenly as possible. This faster mixing step (Stage 1) is followed by a

228     slower mixing step (Stage 2) for a longer time period to allow for continued floc growth.[55] To

229     test the effect of both mixture speed and vortex flow on the growth of the flocs, four different

230     flow regimes were selected for Stage 1 mixing. A set of laminar flow states with corresponding

231     Taylor and wavy vortex types (LTV and LWV, respectively), and a set of turbulent flow states

232     with corresponding Taylor and wavy vortex types (labeled TTV and TWV, respectively) were

233 used for this study as shown in Figure 2B. The flow states were reported in terms of the inner

234 cylinder Reynolds number, $Re_i$. The Re for TC flow is defined by the following equation

$$Re_i = \frac{\Omega_i R_i d}{\nu} \#(3)$$

235 where $R_i$ and $\Omega_i$ are the inner cylinder radius and rotational speed, respectively, $d$ is the gap width

236 between the inner and outer cylinders, and $\nu$ is the kinematic viscosity of the sample.[56] The Stage

237 2 mixing speed was kept constant for all experiments at $Re$ of 1680 (TWV). For this particular

238 TC cell, the ranges for the flow states in terms of Re are 124 to 167 for LTV, 251 to 870 for

239 LWV, 1400 to 2924 for TWV, and above 2924 for TTV.

240 Figure 3 depicts the time-dependent radius of gyration, $R_g$, for the bentonite flocs as a

241 function of time and vortex flow type. The radius of gyration of the flocs increases in all runs

242 after the initial injection of cationic polyacrylamide at time = 30 seconds, until a plateau value of

243 $R_g$ is obtained. The plateau values of $R_g$ were approximately 1.1 mm in the LWV, TWV, and

244 TTV cases while the plateau value was approximately 0.7 mm in the LTV case. Shear breakage

245 of the flocs due to velocity gradients present in the flow limit the maximum floc size.[6,9,17,45]

246 Interestingly, the curves for the $Re$ of 4150 and 5530 cases show nearly identical growth

247 behavior, most likely due to their having the same vortex type.

248 The floc growth rate can be quantified from the data by using a modified version of the

249 logistic growth equation

$$\frac{R_g(t)}{R_{g,max}} = \frac{1}{1 + \left( \frac{1}{R_{g,0}/R_{g,max}} - 1 \right) e^{-rt}} \#(4)$$

12

250    where $R_g$ is the radius of gyration at a given time in mm, $R_{g,max}$ is the maximum value of $R_g$ in the

251    fitting range in mm, $R_{g,0}$ is the initial value of $R_g$ at the beginning of the fitting range in mm, $r$ is

252    the growth rate in mm/s, and $t$ is time in seconds. While this model is typically used for

253    quantifying growth rates in microbial and ecological studies, it has also been used to quantify

254    floc growth as the flocs tend to reach a "carrying capacity" in their population in the form of a

255    maximum floc size.[57–60]

256         The logistic growth equation was fit to the portion of the plot where there was a marked

257    increase in the floc size with time. The fits to the relevant portion of the data are presented in

258    Figure 4 and Figures S2-S5. In addition to the fits, the residuals between the measured values

259    and calculated values from the logistic growth equation are present to show how well the logistic

260    growth equation fits the data points. For the LWV, TWV, and TTV experiments, the model fits

261    the data well based on the residuals. The model was not a good fit for the LTV experiment based

262    on the residuals. This was most likely due to the relatively poor mass transfer of the polymer

263    flocculant associated with the LTV flow state, which is discussed in the following section.

264         Previous investigations have shown that maximum floc size is on the order of the

265    Kolmogorov microscale, and floc size decreases with increasing global velocity gradient via the

266    global dissipation rate of turbulent kinetic energy.[9,45,61] What was interesting to note about the

267    floc size results from the present study is that maximum floc size did not differ much between

268    the different inner cylinder speeds with the exception of the lowest speed. Prior flocculation

269    studies in the literature, however, explored mixing hydrodynamics on flocculation in stirred

270    tanks with impellers or in TC cells under uncontrolled mixing conditions, which have been

271    shown to possess inhomogeneities over spatial and temporal flow features.[10,45]

272        3.2    Effect of Hydrodynamics on Polymer Flocculant Mass Transfer

273        Figure 3 also shows a delay in the growth of the flocs as a function of inner cylinder

274    speed. The lag time is defined as the point in time where the slope of the growth curve

275    instantaneously increased rapidly from zero slope. This delay, or lag time, in growth can be

276    attributed to the intervortex mass transfer of the cationic polyacrylamide. Intervortex mass

277    transfer can be quantified by an effective dispersion coefficient recently determined for this

278    particular TC cell by Wilkinson and Dutcher

$$D_z^* = 2\lambda k_{cb} \#(5)$$

279    where $\lambda$ is the axial wavelength of the vortex, and $k_{cb}$ is the intermixing coefficient.[51,62]

280    Intervortex mass transfer refers to mass transfer of the polyacrylamide between individual vortex

281    bands versus intravortex mass transfer, which refers to mass transfer of the polyacrylamide

282    within a single vortex. To compare the effect of intervortex mixing during the flocculation

283    process, the lag time was plotted against the effective dispersion coefficient for the initial mixing

284    step as shown in Figure 5. The lag times varied from 40 seconds for the highest order flow state

285    (TTV) up to 1600 seconds for the lowest order flow state (LTV). $D_z^*$ increases approximately an

286    order of magnitude from $1.12 \times 10^{-5}$ m$^2$/s to $2.16 \times 10^{-4}$ m$^2$/s over the range of $Re$ used in this

287    study, indicating improved mass transfer of the polymer as the inner cylinder speed increased.

288        The lag time strongly depends on the initial Stage 1 speed.  For the higher mix speeds of

289    $Re$ of 4150 and 5530 cases (TTV), most of the growth curve from Figure *3* is contained within

290    the initial Stage 1 mixing portion of the plot, which are the data to the left of the solid gray line.

291    The growth curve for the $Re$ of 1870 (TWV) begins before the solid gray line in the Stage 1

292    region and continues past the line into the Stage 2 mixing region to the right of the dark gray line.

293    Unlike the turbulent cases, the growth for the $Re$ of 160 (LTV) and $Re$ of 650 (LWV) cases

294    commences well past the speed transition between Stage1 and Stage 2. As the mass and therefore

295    global concentration of polymer injected into the system is consistent across all trials, this

296    difference in the initiation of floc growth is due to the reduced mass transfer abilities of the

297    laminar flow states compared to their corresponding turbulent flow states. The decrease in

298    effective dispersion coefficient and increase in lag time of the LTV and LWV states compared to

299    the TWV and TTV states are therefore largely due to the reduced ability of the LTV flow state to

300    intermix the polymer flocculant with the bentonite to form flocs. In addition to reduced mass

301    transfer abilities based on *Re*, the presence of an "unmixed core" in the laminar flow states

302    observed and discussed previously could also be an explanation for poorer mixing compared to

303    the corresponding TWV flow state.[43,49–51,63] Evidence of this "unmixed core" was not present in

304    the turbulent flow states.

305        3.3    Effect of Hydrodynamics on Floc Morphology

306        In addition to floc size, hydrodynamics play a key role in floc morphology. Solid particulate

307    removal efficiency via sedimentation and filtration depends on the floc structure as morphology

308    is related to both floc size and density.[64] Velocity gradients in the mixing process can alter the

309    floc structure with time, which can also have consequences for removal efficiency. Floc

310    morphology can be quantified using fractal dimensions. Previous studies used light scattering

311    techniques to obtain a mass fractal dimension, which gives three-dimensional information about

312    the floc structure.[11,65,66] However, using light scattering requires removal of sample flocs from

313    their original environment. In order to measure floc structure in a non-intrusive manner, image

314    analysis can be used to calculate a two-dimensional fractal dimension, $D_{sf}$.[10,64,67]

315        The two-dimensional fractal dimension was obtained by linearly regressing a plot of the

316    log of the area versus log of the perimeter for each ten second data set. The closer the $D_{sf}$ value is

15

317    to 1, the more circular the floc is in profile whereas the closer $D_{sf}$ is to 2, the more linear and rod-

318    like the floc is in profile. Figure 6 shows the evolution of $D_{sf}$ with time at each Stage 1 mixing

319    speed. In all cases, $D_{sf}$ decreases with time until $D_{sf}$ plateaus during the later Stage 2 portion of

320    the plot. The plateau value of $D_{sf}$ at the end of the flocculation experiment is largest for the

321    slowest speed ($Re = 160$), and decreases with increasing inner cylinder speed. This decrease in

322    $D_{sf}$ with increasing inner cylinder speed is caused by the larger velocity gradients present in more

323    turbulent flow types (higher speeds), which at longer mixing times shear the edges of the flocs

324    and subsequently round them off.

325        The absence of a particle imaging velocimetry setup (PIV) does not allow for a precise

326    distribution of the velocity gradient. However, a global velocity gradient term at each inner

327    cylinder speed can be calculated using the following equations:

$$G = \sqrt{\frac{\langle \varepsilon \rangle}{\nu}} \#(6)$$

328        where G is the global velocity gradient, $\langle \varepsilon \rangle$ is the global viscous dissipation of the turbulent

329    kinetic energy, and $\nu$ is the kinematic viscosity of the bentonite suspension.[45] The viscous

330    dissipation of turbulent kinetic energy can be calculate using the following equation:

$$\langle \varepsilon \rangle = \nu \left(\frac{dU}{dx}\right)^2 \approx \nu \left(\frac{U_{inner} - U_{outer}}{d}\right)^2 \#(7)$$

331        Where $U_{inner}$ is the angular velocity of the inner cylinder, $U_{outer}$ is the angular velocity of the

332    outer cylinder, and d is the gap width between the two cylinders. Since the outer cylinder is

333    stationary for all experiments, $U_{outer}$ reduces to zero. The global velocity gradient was calculated

16

334     for each Stage 1 mixing speed and are listed here in order of increasing mixing speed: 2.0 s$^{-1}$, 8.6

335     s$^{-1}$, 25.3 s$^{-1}$, 55.7 s$^{-1}$, 74.4 s$^{-1}$. The Stage 2 global velocity gradient is 23.3 s$^{-1}$.

336     During the flocculation process in water treatment, the flocculant is mixed at higher speeds

337     (which implies a higher global velocity gradient) into the suspension to rapidly disperse the

338     flocculant, which subsequently also allows for more aggregate-aggregate collisions to form the

339     initial flocs. Certainly increasing the mixing speed would initially result in aggregates with

340     morphologies that are less circular ($D_{sf}$ values tending toward 2 rather than 1) due to increased

341     aggregate-aggregate collisions from orthokinetic aggregation compared to diffusion alone.[12,67]

342     However, here we should note that with sufficient speeds and mixing times, the $D_{sf}$ values

343     decrease asymptoticly to unity (more circular floc morphology), suggesting that the shear-

344     induced rounding overwhelms aggregate-aggregate collisions in determining floc morphology in

345     turbulent flows at longer mixing times.

346     4     Conclusion

347

348     The unique ability for this TC cell to non-intrusively inject one fluid into another fluid offers

349     unprecedented access to the entire mixing process during flocculation. To summarize the overall

350     effects on flocculation of bentonite clay with cationic polyacrylamide in distilled water at four

351     different flow states generated by the TC cell, the floc growth rate and $D_{sf}$ at the speed transition

352     have been plotted for each inner cylinder speed as shown in Figure 7. As the inner cylinder speed

353     increases, the flocs more rapidly increase in size and become more spherical in shape. The

354     differences in floc growth rate and morphology are largely attributed to the global velocity

355     gradients associated with each flow state, which also affect the dispersion of the polymer

356     flocculant. The intermixing coefficients calculated and shown in Figure 5, which describe

357 turbulent dispersion and not molecular diffusion, of the polyacrylamide in solution are several

358 orders of magnitude larger than the diffusion coefficients of polymers similar to the one used in

359 this study.[68] Even though at the highest speeds tested here the growth rate was the fastest, the

360 fractal dimension of the flocs were more circular, indicating more shear rounding and breakage

361 at the surfaces of the flocs. Based on the results collected in this study, a balance between faster

362 growth rate and shear rounding needs to be met to satisfy the criteria for large, hydrodynamically

363 robust flocs.

364 Flocculation is a largely non-equilibrium process that is dependent on a variety of

365 physicochemical and hydrodynamic properties. The unique ability to directly inject a flocculant

366 into a particulate-laden suspension in this TC cell offers the ability to study the entirety of the

367 flocculation process in a hydrodynamically controlled fashion. While only one type of polymer

368 flocculant was used here and the ionic strength and pH of the water were kept consistent, these

369 process variables critical to the flocculation process can be altered for future experimental

370 studies. Fundamental understanding of the effects of these process variables on flocculation can

371 potentially be used to optimize water treatment operations.

372 5   Conflicts of Interest

373

374 There are no conflicts to declare.

375

376 6   Acknowledgments

388    7    References

389    1    B. Bolto and J. Gregory, Organic polyelectrolytes in water treatment, *Water Res.*, 2007, **41**,
390        2301–2324.

391    2    S. M. R. Shaikh, M. S. Nasser, I. Hussein, A. Benamor, S. A. Onaizi and H. Qiblawey,
392        Influence of polyelectrolytes and other polymer complexes on the flocculation and
393        rheological behaviors of clay minerals: A comprehensive review, *Sep. Purif. Technol.*,
394        2017, **187**, 137–161.

395    3    L. Feng, M. C. Stuart and Y. Adachi, Dynamics of polyelectrolyte adsorption and
396        colloidal flocculation upon mixing studied using mono-dispersed polystyrene latex
397        particles, *Adv. Colloid Interface Sci.*, 2015, **226**, 101–114.

398    4    B. Oyegbile, P. Ay and S. Narra, Introduction Flocculation kinetics and hydrodynamic
399        interactions in natural and engineered flow systems: A review, *Environ. Eng. Res*, 2016,
400        **21**, 1–14.

401    5    J. C. Berg, *An Introduction to Interfaces and Colloids*, World Scientific, 2009.

402    6    Z. Zhu, H. Wang, J. Yu and J. Dou, On the Kaolinite Floc Size at the Steady State of
403        Flocculation in a Turbulent Flow, , DOI:10.1371/journal.pone.0148895.

404    7    Y. Adachi and T. Wada, Initial Stage Dynamics of Bridging Flocculation of Polystyrene
405        Latex Spheres with Polyethylene Oxide, *J. Colloid Interface Sci.*, 2000, **229**, 148–154.

406    8    Y. Adachi and J. Xiao, Initial stage of bridging flocculation of PSL particles induced by
407        an addition of polyelectrolyte under high ionic strength, *Colloids Surfaces A Physicochem.*
408        *Eng. Asp.*, 2013, **435**, 127–131.

409    9    D. Bouyer, C. Coufort, A. Liné and Z. Do-Quang, Experimental analysis of floc size
410        distributions in a 1-L jar under different hydrodynamics and physicochemical conditions,
411        *J. Colloid Interface Sci.*, 2005, **292**, 413–428.

412    10    M. Vlieghe, C. Coufort-Saudejaud, C. Frances and A. Liné, *In situ* characterization of floc
413        morphology by image analysis in a turbulent Taylor-Couette reactor, *AIChE J.*, 2014, **60**,
414        2389–2403.

415    11    Peter Jarvis, A. Bruce Jefferson and S. A. Parsons, Breakage, Regrowth, and Fractal
416        Nature of Natural Organic Matter Flocs, *Environ. Sci. Technol.*, 2005, **39**, 2307–2314.

417    12    W. Yu, J. Gregory, L. Campos and G. Li, The role of mixing conditions on floc growth,
418        breakage and re-growth, *Chem. Eng. J.*, 2011, **171**, 425–430.

419    13    L. Guibai and J. Gregory, Flocculation and sedimentation of high-turbidity waters, *Water*
420        *Res.*, 1991, **25**, 1137–1143.

421    14    S. Biggs, M. Habgood, G. J. Jameson and Y. Yan, Aggregate structures formed via a
422        bridging flocculation mechanism, *Chem. Eng. J.*, 2000, **80**, 13–22.

423    15    Y. Zhou and G. V. Franks, Flocculation Mechanism Induced by Cationic Polymers
424        Investigated by Light Scattering, *Langmuir*, 2006, **22**, 6775–6786.

425    16    I. Szilagyi, G. Trefalt, A. Tiraferri, P. Maroni and M. Borkovec, Polyelectrolyte
426          adsorption, interparticle forces, and colloidal aggregation, *Soft Matter*, 2014, **10**, 2479.

427    17    E. Barbot, P. Dussouillez, J. Y. Bottero and P. Moulin, Coagulation of bentonite
428          suspension by polyelectrolytes or ferric chloride: Floc breakage and reformation, *Chem.*
429          *Eng. J.*, 2010, **156**, 83–91.

430    18    M. G. Rasteiro, I. Pinheiro, F. A. P. Garcia, P. Ferreira and D. Hunkeler, Using Light
431          Scattering to Screen Polyelectrolytes (PEL) Performance in Flocculation, *Polymers*
432          *(Basel).*, 2011, **3**, 915–927.

433    19    N. G. Hoogeveen, M. A. C. Stuart and G. J. Fleer, Polyelectrolyte Adsorption on Oxides: I.
434          Kinetics and Adsorbed Amounts, *J. Colloid Interface Sci.*, 1996, **182**, 133–145.

435    20    M. Rossini, J. G. Garrido and M. Galluzzo, Optimization of the coagulation–flocculation
436          treatment: influence of rapid mix parameters, *Water Res.*, 1999, **33**, 1817–1826.

437    21    J. Roussy, M. Van Vooren, B. A. Dempsey and E. Guibal, Influence of chitosan
438          characteristics on the coagulation and the flocculation of bentonite suspensions, *Water*
439          *Res.*, 2005, **39**, 3247–3258.

440    22    N. Levy, S. Magdassi and Y. Bar-Or, Physico-chemical aspects in flocculation of
441          bentonite suspensions by a cyanobacterial bioflocculant, *Water Res.*, 1992, **26**, 249–254.

442    23    S. M. Shaikh, M. Nasser, I. A. Hussein and A. Benamor, Investigation of the effect of
443          polyelectrolyte structure and type on the electrokinetics and flocculation behavior of
444          bentonite dispersions, *Chem. Eng. J.*, 2017, **311**, 265–276.

445    24    G. Waajen, F. Van Oosterhout, G. Douglas and M. Lürling, Management of
446          eutrophication in Lake De Kuil (The Netherlands) using combined flocculant e
447          Lanthanum modified bentonite treatment, , DOI:10.1016/j.watres.2015.11.034.

448    25    J. D. G. Durán, M. M. Ramos-Tejada, F. J. Arroyo and F. González-Caballero,
449          Rheological and Electrokinetic Properties of Sodium Montmorillonite Suspensions, *J.*
450          *Colloid Interface Sci.*, 2000, **229**, 107–117.

451    26    A. Cadene, S. Durand-Vidal, P. Turq and J. Brendle, Study of individual Na-
452          montmorillonite particles size, morphology, and apparent charge, *J. Colloid Interface Sci.*,
453          2005, **285**, 719–730.

454    27    M. S. Żbik, D. J. Williams, Y.-F. Song and C.-C. Wang, The formation of a structural
455          framework in gelled Wyoming bentonite: direct observation in aqueous solutions., *J.*
456          *Colloid Interface Sci.*, 2014, **435**, 119–27.

457    28    J. Stawiński, Influence of Calcium and Sodium Concentration on the Microstructure of
458          Bentonite and Kaolin, *Clays Clay Miner.*, 1990, **38**, 617–622.

459    29    C. S. Lee, J. Robinson and M. F. Chong, A review on application of flocculants in
460          wastewater treatment, *Process Saf. Environ. Prot.*, 2014, **92**, 489–508.

461    30    P. T. Spicer, W. Keller and S. E. Pratsinis, The Effect of Impeller Type on Floc Size and
462          Structure during Shear-Induced Flocculation, *J. Colloid Interface Sci.*, 1996, **184**, 112–

463  122.

464 31 S. D. T. Axford and T. M. Herrington, Determination of aggregate structures by combined
465   light-scattering and rheological studies, *J. Chem. Soc. Faraday Trans.*, 1994, **90**, 2085.

466 32 G. C. Bushell, Y. D. Yan, D. Woodfield, J. Raper and R. Amal, On techniques for the
467   measurement of the mass fractal dimension of aggregates, *Adv. Colloid Interface Sci.*,
468   2002, **95**, 1–50.

469 33 J. A. Rice, E. Tombácz and K. Malekani, Applications of light and X-ray scattering to
470   characterize the fractal properties of soil organic matter, *Geoderma*, 1999, **88**, 251–264.

471 34 M. Soos, L. Ehrl, M. U. Bäbler and M. Morbidelli, Aggregate breakup in a contracting
472   nozzle., *Langmuir*, 2010, **26**, 10–8.

473 35 C. D. Andereck, S. S. Liu and H. L. Swinney, Flow regimes in a circular Couette system
474   with independently rotating cylinders, *J. Fluid Mech.*, 2006, **164**, 155.

475 36 C. S. Dutcher and S. J. Muller, Explicit analytic formulas for Newtonian Taylor-Couette
476   primary instabilities., *Phys. Rev. E. Stat. Nonlin. Soft Matter Phys.*, 2007, **75**, 047301.

477 37 C. S. Dutcher and S. J. Muller, Spatio-temporal mode dynamics and higher order
478   transitions in high aspect ratio Newtonian Taylor–Couette flows, *J. Fluid Mech.*, 2009,
479   **641**, 85.

480 38 M. A. Fardin, C. Perge and N. Taberlet, "The hydrogen atom of fluid dynamics" –
481   introduction to the Taylor–Couette flow for soft matter scientists, *Soft Matter*, 2014, **10**,
482   3523.

483 39 M. S. Zbik, R. S. C. Smart and G. E. Morris, Kaolinite flocculation structure, *J. Colloid*
484   *Interface Sci.*, 2008, **328**, 73–80.

485 40 M. V. Majji, S. Banerjee and J. F. Morris, Inertial flow transitions of a suspension in
486   Taylor–Couette geometry, *J. Fluid Mech.*, 2018, **835**, 936–969.

487 41 C. S. Dutcher and S. J. Muller, The effects of drag reducing polymers on flow stability :
488   Insights from the Taylor-Couette problem, *Korea-Australia Rheol. J.*, 2009, **21**, 213–233.

489 42 C. S. Dutcher and S. J. Muller, Effects of moderate elasticity on the stability of co- and
490   counter-rotating Taylor–Couette flows, *J. Rheol. (N. Y. N. Y).*, 2013, **57**, 791.

491 43 M. Nemri, S. Charton and E. Climent, Mixing and axial dispersion in Taylor–Couette
492   flows: The effect of the flow regime, *Chem. Eng. Sci.*, 2016, **139**, 109–124.

493 44 N. Tilton, D. Martinand, E. Serre and R. M. Lueptow, Pressure-driven radial flow in a
494   Taylor–Couette cell, *J. Fluid Mech.*, 2010, **660**, 527–537.

495 45 C. Coufort, D. Bouyer and A. Liné, Flocculation related to local hydrodynamics in a
496   Taylor–Couette reactor and in a jar, *Chem. Eng. Sci.*, 2005, **60**, 2179–2192.

497 46 C. Selomulya, G. Bushell, R. Amal and T. D. Waite, Aggregate properties in relation to
498   aggregation conditions under various applied shear environments, *Int. J. Miner. Process.*,
499   2004, **73**, 295–307.

500  47   L. Guérin, C. Coufort-Saudejaud, A. Liné and C. Frances, Dynamics of aggregate size and
501       shape properties under sequenced flocculation in a turbulent Taylor-Couette reactor, *J.*
502       *Colloid Interface Sci.*, 2017, **491**, 167–178.

503  48   N. Wilkinson and C. S. Dutcher, Taylor-Couette flow with radial fluid injection, *Rev. Sci.*
504       *Instrum.*, 2017, **88**, 083904.

505  49   M. Nemri, E. Climent, S. Charton, J.-Y. Lanoë and D. Ode, Experimental and numerical
506       investigation on mixing and axial dispersion in Taylor–Couette flow patterns, *Chem. Eng.*
507       *Res. Des.*, 2013, **91**, 2346–2354.

508  50   M. Nemri, S. Cazin, S. Charton and E. Climent, Experimental investigation of mixing and
509       axial dispersion in Taylor–Couette flow patterns, *Exp. Fluids*, 2014, **55**, 1769.

510  51   N. Wilkinson and C. S. Dutcher, Axial Mixing and Vortex Stability to in-situ Radial
511       Injection in Taylor-Couette Laminar and Turbulent Flows, *J. Fluid Mech., accepted.*

512  52   S. Kaufhold, R. Dohrmann, D. Koch and G. Houben, The pH of Aqueous Bentonite
513       Suspensions, *Clays Clay Miner.*, 2008, **56**, 338–343.

514  53   N. Wilkinson, A. Metaxas, E. Brichetto, S. Wickramaratne, T. M. Reineke and C. S.
515       Dutcher, Ionic strength dependence of aggregate size and morphology on polymer-clay
516       flocculation, *Colloids Surfaces A Physicochem. Eng. Asp.*, 2017, **529**, 1037–1046.

517  54   N. Wilkinson, A. Metaxas, C. Quinney, S. Wickramaratne, T. M. Reineke and C. S.
518       Dutcher, pH dependence of bentonite aggregate size and morphology on polymer-clay
519       flocculation, *Colloids Surfaces A Physicochem. Eng. Asp.*, 2018, **537**, 281–286.

520  55   M. A. Yukselen and J. Gregory, The effect of rapid mixing on the break-up and re-
521       formation of flocs, *J. Chem. Technol. Biotechnol.*, 2004, **79**, 782–788.

522  56   G. S. Lewis and H. L. Swinney, Velocity structure functions, scaling, and transitions in
523       high-Reynolds-number Couette-Taylor flow, *Phys. Rev. E*, 1999, **59**, 5457–5467.

524  57   F. Kargi, Re-interpretation of the logistic equation for batch microbial growth in relation
525       to Monod kinetics, *Lett. Appl. Microbiol.*, 2009, **48**, 398–401.

526  58   Y. V. Bukhman, N. W. DiPiazza, J. Piotrowski, J. Shao, A. G. W. Halstead, M. D. Bui, E.
527       Xie and T. K. Sato, Modeling Microbial Growth Curves with GCAT, *BioEnergy Res.*,
528       2015, **8**, 1022–1030.

529  59   D. Mikeš, A Simple Floc-Growth Function for Natural Flocs in Estuaries, *Math Geosci*,
530       2011, **43**, 593–606.

531  60   H.-Q. Su, Kui-Zu and Yu, Formation and Characterization of Aerobic Granules in a
532       Sequencing Batch Reactor Treating Soybean-Processing Wastewater, *Environ. Eng. Sci.*,
533       2005, **39**, 2818–2827.

534  61   D. Bouyer, A. Liné and Z. Do-Quang, Experimental analysis of floc size distribution
535       under different hydrodynamics in a mixing tank, *AIChE J.*, 2004, **50**, 2064–2081.

536  62   N. Ohmura, K. Kataoka, Y. Shibata and T. Makino, Effective mass diffusion over cell
537       boundaries in a Taylor-Couette flow system, *Chem. Eng. Sci.*, 1997, **52**, 1757–1765.

538  63  J. Dusting and S. Balabani, Mixing in a Taylor–Couette reactor in the non-wavy flow
539      regime, *Chem. Eng. Sci.*, 2009, **64**, 3103–3111.

540  64  P. T. Spicer, W. Keller and S. E. Pratsinis, The Effect of Impeller Type on Floc Size and
541      Structure during Shear-Induced Flocculation, *J. Colloid Interface Sci.*, 1996, **184**, 112–
542      122.

543  65  T. Li, Z. Zhu, D. Wang, C. Yao and H. Tang, Characterization of floc size, strength and
544      structure under various coagulation mechanisms, *Powder Technol.*, 2006, **168**, 104–110.

545  66  T. Li, Z. Zhu, D. Wang, C. Yao and H. Tang, The strength and fractal dimension
546      characteristics of alum–kaolin flocs, *Int. J. Miner. Process.*, 2007, **82**, 23–29.

547  67  Z. Zhu, J. Yu, H. Wang, J. Dou and C. Wang, Fractal Dimension of Cohesive Sediment
548      Flocs at Steady State under Seven Shear Flow Conditions, *Water*, 2015, **7**, 4385–4408.

549  68  B. Tinland, A. Pluen, J. Sturm and G. Weill, *Persistence Length of Single-Stranded DNA*,
550      1997.

551

552

553
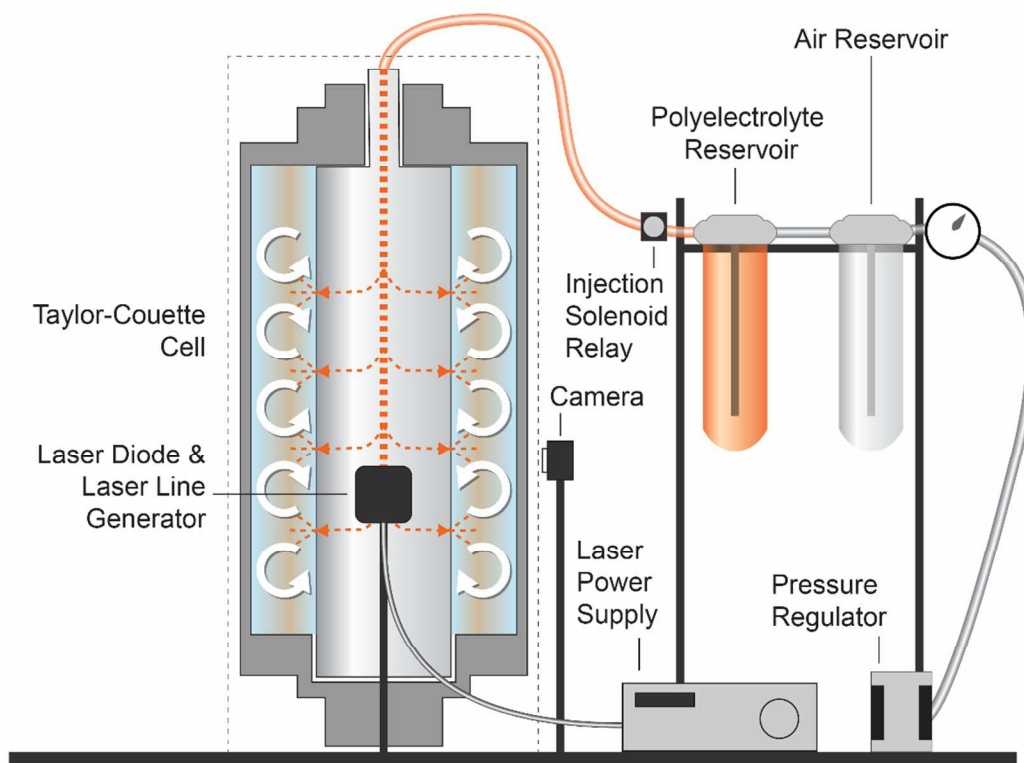
554   8   Figures

555

556   Figure 1: Experimental set-up for flocculation experiments in the TC cell. The bentonite
557   suspension is loaded into the annulus by way of tubing attached to a Swagelok valve attached to
558   the bottom of the cylinder base. The polyelectrolyte is held in a reservoir as pictured here and is
559   injected at the top of the inner cylinder by way of a solenoid valve, which is controlled by a
560   LabView program. The stepper motor for the inner cylinder is controlled separately by a motor
561   controller. Under normal operating conditions, the Plexiglass tank surrounding the TC cell is
562   filled with paraffin oil to match the index of refraction of the glass outer cylinder, which
563   eliminates its curved surface during recording.

564

565

566

567

568

569

570

571

572

573

574



575
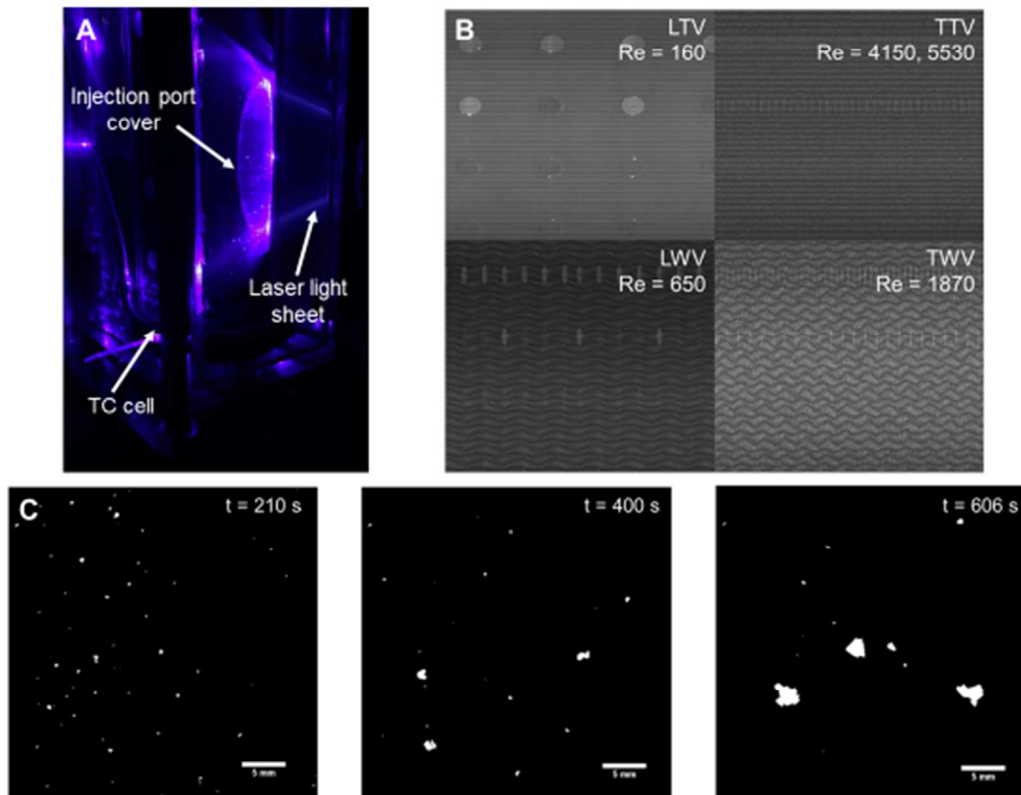
Figure 2: A) Laser light sheet generated from laser diode illuminating the injection port cover and bentonite flocs. B) The four wave states with their vortex type and speed in terms of Re. There are two laminar types (Laminar Taylor Vortex, LTV and Laminar Wavy Vortex, LWV) and two turbulent types (Turbulent Taylor Vortex, TTV and Turbulent Wavy Vortex, TWV). The gray circles present in the image are the injection port covers. C) Binarized images of bentonite flocs from at 210 s, 400 s, and 606 s into flocculation at an inner cylinder Growth Speed of $Re = 4150$. Scale bars in C) are all 5 mm in length.

583

584

585

586

587

588

589

590

591



592
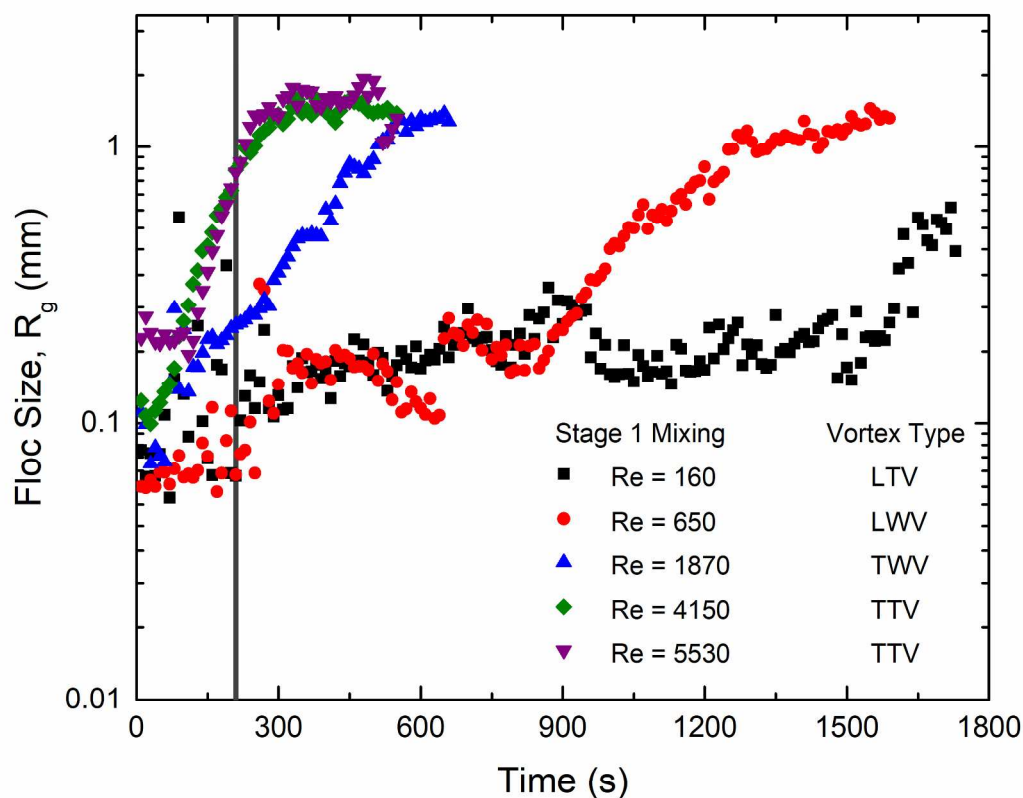
Figure 3: Bentonite floc size as a function of time and Stage 1 mixing speed in terms of the inner
cylinder rotational speed. The corresponding vortex type is listed next to the speed. The vertical,
dark gray line denotes the point in time where the speed changes from the Stage 1 speed to Stage
2 speed, which is held constant for all experiments at 0.46 s$^{-1}$. Each point represents data
averaged from 300 frames of the movie (10 s at a frame rate of 30 fps).

598

599

600

601

602

603

604

605

606



607
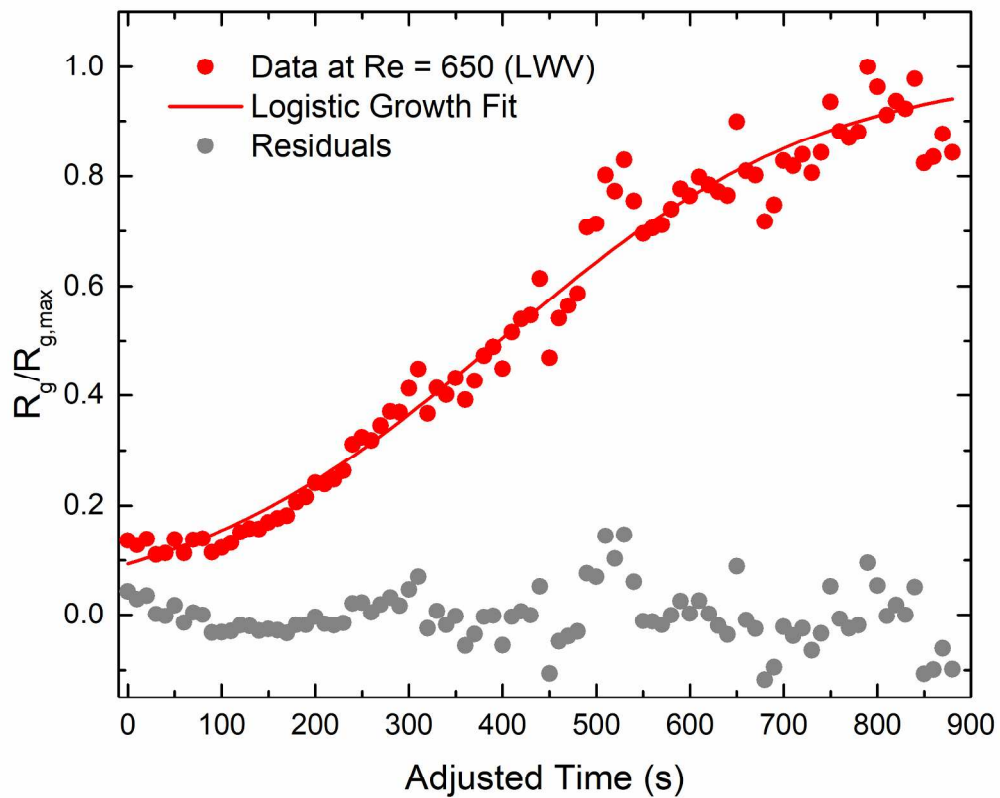
Figure 4: Logistic growth fit to floc size data at inner cylinder speed of 0.17 s$^{-1}$ (Re = 650, LWV) over time. The red dots represent the $R_g$ data points collected during the experiment normalized by the maximum value of $R_g$ in the fitting range. The red line indicates the fit. The gray data points are the residuals of the fit, which is the data point calculated by the logistic growth model subtracted from the original data at the corresponding time point.

613

614

615

616

617

618

619

620

621



622
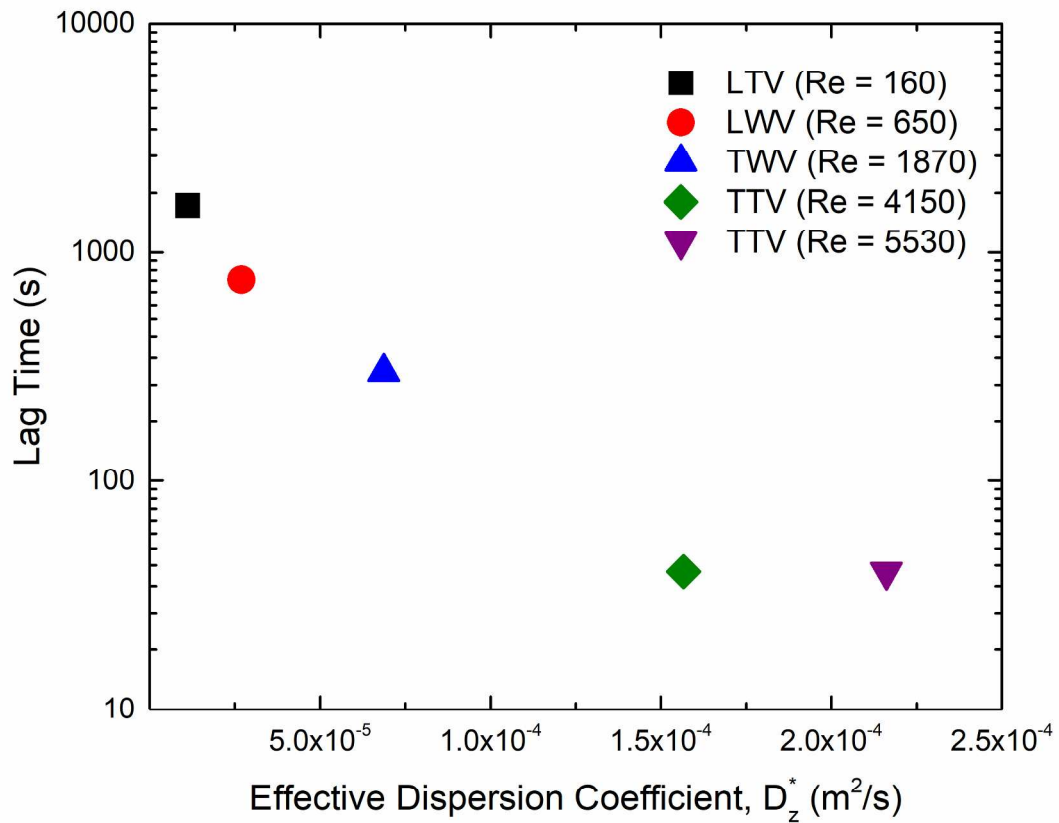
Figure 5: Lag time of floc growth verse the effective dispersion coefficient, $D_z^*$. Lag time refers to the point in time during flocculation where the flocs commence growth.
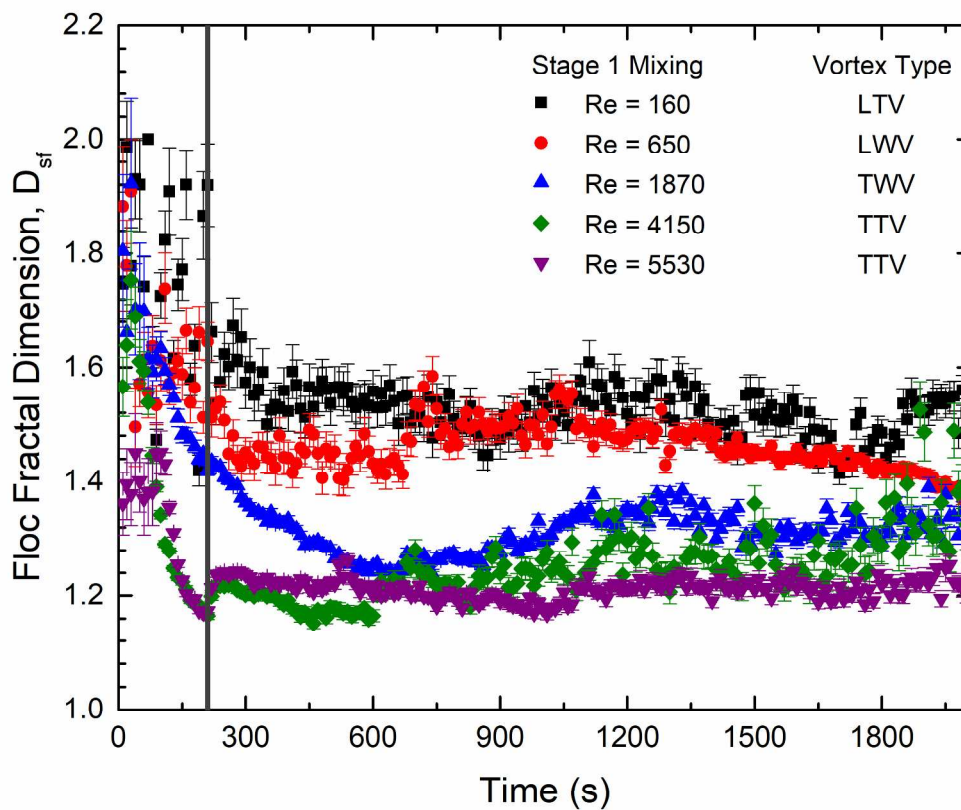
625

626

627

628

629

630

631

632

633

634

635



636

Figure 6: Bentonite morphology quantified as a 2-D perimeter-based fractal dimension as a function of time and Stage 1 mixing speed. The corresponding vortex type is listed next to the speed. The vertical, dark gray line denotes the point in time where the speed changes from the Mix Speed to the Growth Speed, which is held constant for all experiments at $0.46$ s$^{-1}$. Each point represents data averaged from 300 frames of the movie (10 sec at a frame rate of 30 fps).

642

643

644

645

646

647

648

649

650



651
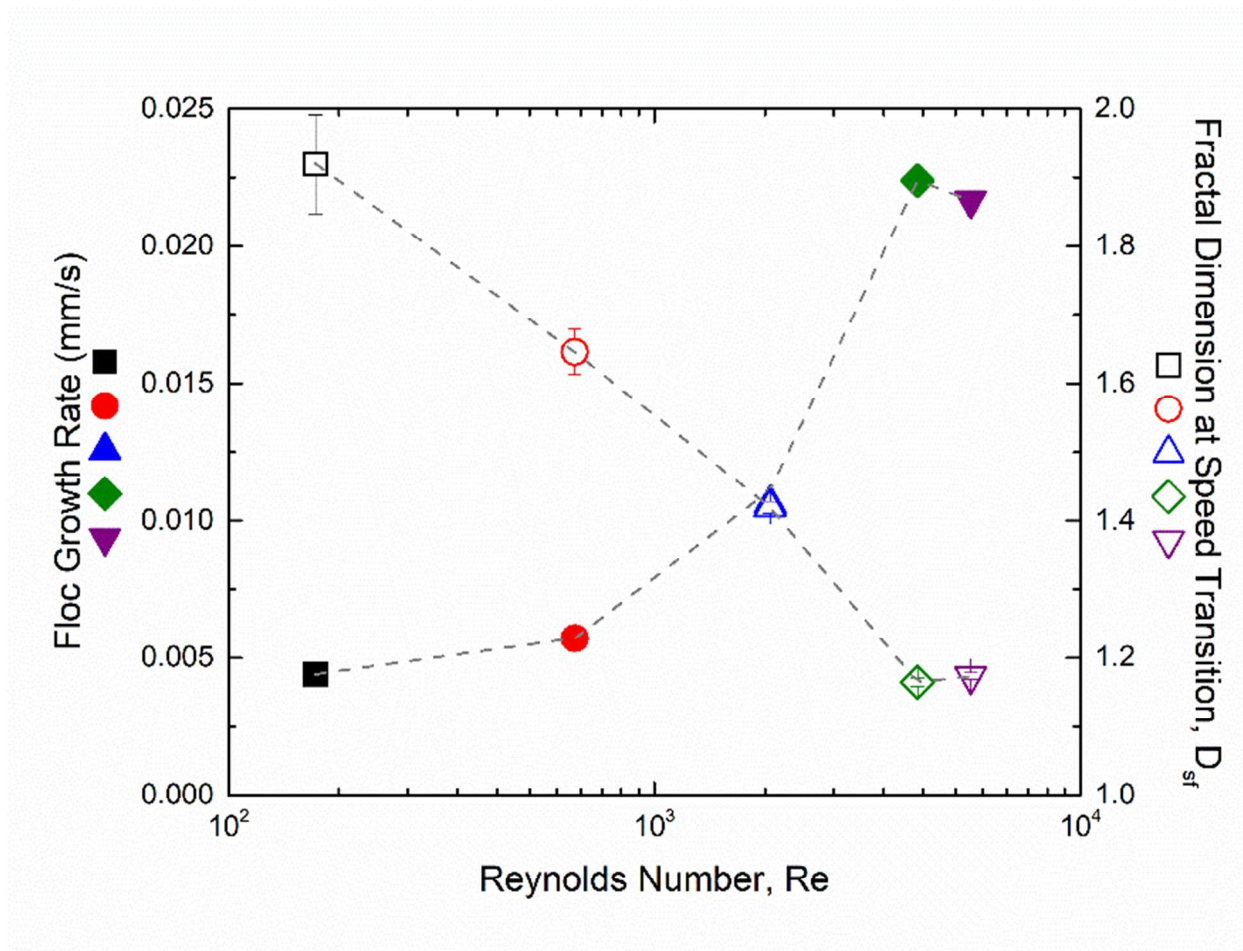
Figure 7: Summary of floc growth rate (closed symbols) and floc fractal dimension (open symbols) as functions of inner cylinder speed. The error bars on the floc fractal dimension represent a 95% confidence interval, and the points were taken at the speed transition between the "Mix Speed and the "Growth Speed." The gray dashed line is there to guide the eye to observe the increasing trend in flow growth rate and decreasing floc fractal dimension with increasing *Re*. The solid blue triangle is behind the open blue triangle. Several of the error bars are obscured by the symbols.